Molecular Therapy - Nucleic Acids

Uptake/activity relationship of fully chemically modified siRNAs in human mononuclear immune cells

--Manuscript Draft--

Manuscript Number:	MTNA-D-23-00254
Full Title:	Uptake/activity relationship of fully chemically modified siRNAs in human mononuclear immune cells
Article Type:	Research Article
Keywords:	siRNA; PBMC; T cell; cell therapy; myeloid cells; Extracellular vesicles; lipid nanoparticles; delivery
Order of Authors:	Anastasia Kremer, MSc
	Tatyana Ryaykenen, MSc
	Reka Agnes Haraszti, MD PhD
Abstract:	Immune cells have been historically difficult to treat with RNA-based medicines due to delivery challenges. At the same time precise modulation of immune cell phenotypes represents an unmet clinical need in various cancers, autoimmune diseases and in cell therapy optimization. Recent data demonstrate that full chemical optimization of siRNAs is indispensable for in vivo preclinical and clinical applications. Furthermore, conjugates and formulations may modulate siRNA pharmacokinetics to reach extrahepatic tissues in therapeutic concentrations. Here we show that lipid-conjugate-mediated delivery outperforms lipid-nanoparticle-mediated and extracellular-vesicle-mediated in human primary T cells ex vivo. Furthermore, lipid-conjugates enable efficient siRNA delivery to further eight immune cell types, including both lymphoid and myeloid lineages. Intracellular siRNA concentration and silencing efficiency have been shown to tightly correlate in various cell types and for various delivery methods both in vitro and in vivo. Surprisingly, uptake and silencing efficiencies show no correlation in a subset of human immune cell types. Kinetics data confirm the cell-type-dependency of uptake mechanisms. Data presented here provide the first step towards immune-cell-type-specific platform construction of immunomodulatory, RNA-based precision medicines.

Uptake/activity relationship of fully chemically modified siRNAs in human mononuclear immune cells

Kremer A[1,2], Ryaykenen T[1,2], Haraszti RA[1,2]

[1] Department of Internal Medicine II, Hematology, Oncology, Clinical Immunology and Rheumatology, University Hospital Tuebingen

[2]Gene and RNA Therapy Center (GRTC), Faculty of Medicine, University Tuebingen

Correspondence should be addressed to: reka.haraszti@med.uni-tuebingen.de

Abstract

Immune cells have been historically difficult to treat with RNA-based medicines due to delivery challenges. At the same time precise modulation of immune cell phenotypes represents an unmet clinical need in various cancers, autoimmune diseases and in cell therapy optimization. Recent data demonstrate that full chemical optimization of siRNAs is indispensable for in vivo preclinical and clinical applications. Furthermore, conjugates and formulations may modulate siRNA pharmacokinetics to reach extrahepatic tissues in therapeutic concentrations. Here we show that lipid-conjugate-mediated delivery outperforms lipid-nanoparticle-mediated and extracellular-vesicle-mediated in human primary T cells ex vivo. Furthermore, lipid-conjugates enable efficient siRNA delivery to further eight immune cell types, including both lymphoid and myeloid lineages. Intracellular siRNA concentration and silencing efficiency have been shown to tightly correlate in various cell types and for various delivery methods both in vitro and in vivo. Surprisingly, uptake and silencing efficiencies show no correlation in a subset of human immune cell types. Kinetics data confirm the cell-type-dependency of uptake mechanisms. Data presented here provide the first step towards immune-cell-type-specific platform construction of immunomodulatory, RNA-based precision medicines.

Introduction

Hyperactivation of specific immune cell subsets and/or pathways drive hematological malignancies and autoimmune diseases or underly failure of cell therapeutics (i.e. CAR T cells). Current therapeutics often fail to specifically target disease driver pathways and co-inhibit numerous pathways in numerous cell subsets instead[1-3]. Approved therapies often inhibit surrogate targets when the disease specific target is undruggable[4, 5]. Both strategies lead to significant toxicities or primary treatment failure. Precision targeting, therefore, is urgently needed to enhance safety and efficacy of therapies for hematological and immunological diseases.

siRNAs, a novel precision medicine drug class, hold promise to meet this clinical need by precisely inhibiting any sequence (including noncoding sequences[6]) in a transcriptome. However, siRNA delivery to immune cells (i.e. effector cells of most hematological and autoimmune diseases) has proved challenging. Electroporation[7], lipid-conjugates[8, 9], aptamer-conjugates[10, 11], antibody-conjugates[12-15] and lipid nanoparticles[16] have shown varying extent of siRNA delivery to T cells ex vivo and/or in vivo. A significant subset of these studies has used unmodified or partially chemically modified siRNAs. Later on, however, all clinical trials using unmodified RNA-based medicines have failed due to inefficiency[17] or toxicity[18] and only one partially modified siRNA has been approved[19]. Accumulating data show the indispensability of full chemical modification of siRNAs in in vivo and clinical applications instead[20]. Since full chemical modification of siRNAs may alter the efficiency of above delivery methods[21], T cell delivery optimization needs to be revisited using fully chemically modified siRNAs. Even though previous siRNA delivery work concentrated mostly on T cells among immune cells[22], many more immune cell types have been shown to drive disease[23] or are explored as cell therapeutic candidates [24-28]. Thus, further delivery optimization is needed for the extended family of immune cells.

Here we evaluate uptake and activity of lipid-conjugated, fully chemically modified siRNAs to a panel of primary human immune cell types. We test lymphoid (T cells, B cells, NK cells) and myeloid (monocytes, macrophages, dendritic cells) cell types commonly involved in leukemias, lymphomas, autoimmune disorders and/or used as cell therapeutics (i.e. CAR T cells[29], donor lymphocyte infusions[30], CAR NK cells[24], CAR macrophages[25], CAR monocytes[26], dendritic cell-based[27] or monocyte-based vaccines[28]). We compare cholesterol-siRNA with two novel lipid-conjugated siRNAs (monovalent-myristic-acid-siRNA and divalent-myristic-acid-siRNAs) that have shown an increased accumulation in mouse primary immune organs: spleen and thymus [31].

Furthermore, we systematically compare available siRNA delivery methods to human T cells using the above lipid-conjugated siRNAs, T-cell-specific lipid nanoparticles[32] and extracellular vesicles derived from mesenchymal stem cells[33].

Results

Cholesterol- and divalent-myristic-acid-conjugates drive efficient siRNA uptake in peripheral blood mononuclear cell types

We screened a panel of lipid conjugated siRNAs for uptake into various human immune cells types. siRNAs were fully chemically modified using a combination of 2´-OMe, 2´-F and phosphorothioates (Supplementary Table 1)[20]. siRNAs were asymmetric with antisense strand of 20 nucleotides long and sense strand 15 nucleotides long in order to facilitate cellular uptake[21]. Cy3 fluorescent label was conjugated to the 5`end of the sense strand and lipids (cholesterol, one or two myristic acids) were covalently conjugated to the 3`end of the sense strand using amino C7 linker as described before[31]. In addition, the 5´phosphate of the antisense strand was stabilized via 5´vinylphosphonate[34].

We isolated T cells, B cells, NK cells, dendritic cells and monocytes from human buffy coat derived peripheral mononuclear cells (PBMCs) using negative selection. We furthermore differentiated macrophages and dendritic cells from monocytes using IL-4, GM-CSF and M-CSF, respectively.

Following 24 hours of co-incubation we observed efficient siRNA uptake into Jurkats (human T cell leukemia cell line), as well as all human primary mononuclear cell types (Fig.1.) as well as in CAR T cells NK-92-MI cell line (Supp.Fig.2.) Cholesterol-siRNA and divalent-myristic-acid-siRNA showed the best uptake efficiency across all cell types tested (Fig.1). In PBMC lymphocyte fraction, which consisted 74 % of resting T cells (Supp. Fig. 1.), in NK cells and in macrophages cholesterol-siRNA outperformed divalent-myristic-acid-siRNA. Interestingly, unconjugated siRNA and monovalent-myristic-acid-siRNA showed almost equally efficient uptake despite monovalent-myristic-acid-siRNA being more hydrophobic [31]. Dendritic cells in blood have two populations representing plasmacytoid and myeloid cells. These two populations demonstrate differential siRNA uptake, generally with cholesterol-siRNA showing the best efficiency. On the contrary, in monocyte derived DCs we see divalent-myristic-acid-siRNA showing slightly better uptake efficiency than cholesterol-siRNA, with cells showing a broad distribution of siRNA fluorescence. Interestingly, unconjugated siRNA also showed robust uptake in all cell types tested.

siRNA uptake and silencing efficiencies do not correlate in peripheral blood mononuclear cell types

To assess how siRNA uptake translates to silencing activity, we treated above immune cells with a dilution series of lipid conjugated siRNAs for 6 days and quantified target mRNA expression.

Interestingly, cholesterol-siRNA and divalent-myristic-acid-siRNA differed in silencing activity in a cell type specific manner (Fig.2.), while showing nearly identical cellular uptake efficiency throughout the immune cell types tested (Fig.1.). Thus, cellular uptake efficiency did not correlate with silencing activity.

Cholesterol-siRNA outperformed divalent-myristic-acid-siRNA in dendritic cells (both enriched from blood p= 0.0065 Fig. 2F and monocyte-derived p=0,0002, Fig.2H) and in PBMC lymphocyte fraction (p=0.0001, Fig.2B) consisting of 74% resting T cells (Supp Fig.1). The activity of divalent-myristic-acid-siRNA improved substantially upon activation of T cells reflected in silencing identical to cholesterol-siRNA in activated T cells (Fig.2.C.). Cholesterol-siRNA and divalent-myristic-acid-siRNA were further

equivalent in Jurkats, NK cells, B cells, monocytes and monocyte-derived macrophages (Fig.2.A, E, D, G, I, respectively).

Even though monovalent-myristic-acid-siRNA showed lower uptake than divalent-myristic-acid-siRNA throughout all cell types (Fig.1.) this was only reflected in silencing in Jurkats ($p= 0.01$), activated T cells ($p=0.003$) and B cells ($p=0.02$). Unexpectedly, in all other cell types tested the two myristic acid siRNA versions did not differ significantly.

Cholesterol-siRNA showed substantially more uptake than unconjugated siRNA throughout tested cell types. Yet, only in T cells (both resting and activated T cells) and in monocytes is this reflected in silencing ($p <0.0001$). In all other cells, cholesterol-sIRNA and unconjugated-siRNA perform similarly (Fig. 2.).

We observed indistinguishable silencing activity of all siRNAs tested in monocyte derived macrophages (Fig.2.F.), reflecting the general phagocytotic nature of this cell type.

Hydrophobicity of lipid conjugated siRNA (cholesterol-siRNA and divalent-myristic-acid-siRNA with roughly the same hydrophobicity, followed by monovalent-myristic-acid-siRNA and unconjugated siRNA [31, 35]) predicted cellular uptake (Fig.1.) but not silencing efficiency (Fig.2.) in peripheral blood mononuclear cells. Instead, lipid conjugate identity defined the silencing activity in a cell type specific manner and enabled up to 200-fold silencing enhancement within one cell type (Fig.2.J.). Possible explanations include differences in the uptake mechanism, intracellular trafficking pathways, endosomal release or metabolism.

Lipid conjugate identity defines siRNA uptake kinetics

Different uptake mechanisms may associate to different uptake kinetics. Therefore, we used flow cytometry in time series experiments to assess uptake kinetics of the two equally hydrophobic compounds, cholesterol-siRNA and divalent-myristic-acid-siRNA (Fig.3.). We used T cell types where different (PBMCs) as well as equal (Jurkats and activated T cells) silencing activity of above compounds has been observed. Indeed, uptake kinetics correlated with silencing activity, cholesterol-siRNA

showing faster uptake than divalent-myristic-acid-siRNA (half time 4,3 hours versus 21,1 hours, respectively, p=0,02) in PBMCs (Fig.3.B.) but not in Jurkats (Fig.3.A.) or in activated T cells (Fig.3.C.). Cholesterol-siRNA uptake reached saturation after 24 hours, while divalent-myristic-acid-siRNA only after 4 days in PBMCs (Fig.3.B.). These data suggest that late uptake may not be productive. Additionally, in activated T cells a decrease in fluorescence signal followed saturation (Fig.3.C.) – potentially suggesting metabolism of the fluorescent tag and/or the entire siRNA. Peak fluorescence during siRNA uptake in activated T cells was nearly triple than that in Jurkats and double than that in PBMCs and correspondingly, the benefit of a lipid conjugate was the largest in activated T cells (Fig.3.) Since PBMC lymphocyte fraction consists of 74 % resting T cells (Supp.Fig.1.), above data may collectively indicate an siRNA uptake mechanism change or shift during T cell activation.

The mechanism of uptake saturation may include (1) insufficient extracellular siRNA concentration, or (2) a limit to the number of intracellular siRNA molecules. To test these hypotheses, we first quantified Cy3 fluorescence remaining in the medium during above time series uptake experiments (Supp. Fig. 3.). We observed a modest decrease in fluorescence in the medium during 4 days of (Supp. Fig. 3.A.). We then added equimolar concentration of fluorescent siRNA 24 hours after initial treatment. Rapid additional uptake of siRNA could be observed, followed by a new saturation phase (Supp. Fig. 3.B-D.). These data suggest that extracellular rather than intracellular siRNA concentration limits the uptake of both cholesterol-siRNA and divalent-myristic-acid-siRNA.

We then used fluorescent microscopy to compare the intracellular localization of cholesterol-siRNA and divalent-myristic-acid-siRNA upon cellular uptake. We chose primary dendritic cells – a cell type with larger cytoplasm than that of T cells and where silencing activity of cholesterol-siRNA and divalent-myristic-acid-siRNA differed profoundly – for imaging studies. Both unconjugated siRNA and divalent-myristic-acid-siRNA showed a granulated fluorescent pattern in the perinuclear region (Fig.4.A.), whereas cholesterol-siRNA was associated to a more confluent perinuclear fluorescent pattern throughout the timepoints. We further observed an increase in the fluorescent pattern confluency and fluorescence intensity in both cholesterol-siRNAs- and divalent-myristic-acid-siRNA-

treated cells (Fig.4.A.). Quantification of fluorescence confirmed an early uptake benefit of cholesterol-siRNA over divalent-myristic-acid-siRNA (Fig.4.B.).

Lipid-conjugate-mediated siRNA delivery outperform nanoparticle-mediated delivery in T cells

Lipid nanoparticles (LNPs) [36] as well as small extracellular vesicles (sEVs) [37] have been successfully used in siRNA delivery in various cell types. Recently, lipid nanoparticles have been developed for RNA delivery specifically to T cells [38]. In addition, extracellular vesicles have been shown to be therapeutic in some T cell mediated diseases [39], partially attributed to small RNA delivery capacity [40].

Therefore, we next asked whether T cell specific LNPs or mesenchymal stem cell derived sEVs could improve lipid-conjugated-siRNA activity in primary human T cells. We used LNPs originally developed for mRNA delivery to T cells as well as small extracellular vesicles purified from umbilical cord matrix mesenchymal stem cells. LNPs and sEVs had a diameter of approximately 100 nm on average (Supp.Fig.4.A-D.) and a slightly negative charge (Supp.Fig.4.E.). and Surprisingly, LNP and sEV mediated delivery showed no benefit in silencing activity compared to unassisted delivery of lipid-conjugated-siRNAs. Unassisted delivery performed best for cholesterol-siRNA (Fig.5.A.) and monovalent-myristic-acid-siRNA (Fig.5.B.), whereas unassisted and sEV mediated delivery was indistinguishable for divalent-myristic-acid-siRNA (Fig.5.C.). LNP mediated delivery performed the poorest for cholesterol-siRNA (Fig.5.A.) and for divalent-myristic-acid-siRNA (Fig.5.C.), whereas LNP mediated and sEV mediated delivery were comparable for monovalent-myristic-acid-siRNA (Fig.5.B.). It remains yet to be elucidated whether LNP and/or sEV mediated delivery leads to a benefit in functional assays.

Discussion

Data presented here demonstrate a discrepancy between cellular uptake and silencing efficiency in several immune cell types. We postulate that lipid-conjugated-siRNAs interact with the cell membrane as well as membranes of the endosomal system. This membrane-siRNA interaction will guide possible intracellular trafficking pathways towards either endosomal release and RISC loading (productive trafficking), endosomal depot formation enabling long effect durations[41] or

degradation/inactivation. Likely, the proportion of lipid-conjugated siRNA distributed to each of these three pathways is defined via the siRNA-membrane interactions. Since membrane composition may largely differ between cell types [42], both the cell type and the lipid-conjugate will alter productive silencing.

Cellular uptake mechanisms of asymmetric siRNAs used in this study include (1) a phosphorothioate-driven mechanism similar to that of antisense oligonucleotides[21], (2) association to LDL via cholesterol-conjugate[43] in medium and uptake via LDL receptors[44], (3) hydrophobic interaction with the cell membrane[45], or a combination of these. To date the myristic-acid-siRNA uptake mechanism remains unknown. Since myristic acid acts as a lipid anchor to various proteins[46], it can be postulated that hydrophobic interactions contribute to cellular uptake of myristic-acid-siRNA. Furthermore, myristylated proteins can be bound by either heme oxygenase 2[47] or Uncoordinated-119[48], proteins playing roles in T cell signaling[47, 48] and TLR4 signaling[47]. Upregulation of these myristic acid binding proteins upon T cell activation may explain an altered intracellular trafficking and silencing efficiency of myristic-acid-siRNA in activated versus resting T cells. Similarly, numerous cholesterol sensing or metabolizing proteins are altered during T cell activation[49], which may affect the trafficking of cholesterol-siRNA.

Collectively, data presented here indicate that the delivery method needs to be optimized for each cell type separately. Our work represents the first step towards creating a library of delivery platforms to human immune cells.

Our data demonstrate superiority of lipid-conjugate mediated delivery of siRNA to T cells over lipid-nanoparticle mediated and extracellular vesicle mediated delivery ex vivo. This came as a surprise, since lipid nanoparticles are acknowledged to facilitate endosomal release[50, 51] and the doses necessary to achieve an equivalent silencing effect in livers in vivo are up to 100 times lower than those for conjugate-mediated-delivery[52]. The lipid nanoparticles used in this study have originally been developed for mRNA delivery[32]. A major difference is the hydrophobic character of lipid-conjugated, fully chemically modified siRNAs, whereas mRNAs are hydrophilic. Possibly, hydrophobic interactions

between the lipid nanoparticle and hydrophobic siRNAs rather impede endosomal release. Indeed, liposome-mediated delivery of cholesterol-siRNA to neurons is less effective than unassisted delivery[53].

Extracellular vesicles are known to deliver siRNAs to cell types resistant to transfection – such as neurons – and induce enhanced silencing effects compared to both lipid-nanoparticle-mediated-delivery and lipid-conjugate-mediated delivery[33, 37, 53]. Here we confirmed superiority of extracellular vesicles over lipid nanoparticles for siRNA delivery in T cells. Interestingly, extracellular vesicles were more advantageous when delivering divalent-myristic-acid-siRNA than cholesterol-siRNA, even though the two compounds have nearly identical hydrophobicities[31, 35]. These data suggest lipid-specific interactions between the extracellular vesicle membrane and the lipid-conjugate, which may affect intracellular release and RISC loading of siRNA upon uptake.

Extracellular vesicle formulation impeded cholesterol-siRNA activity to a larger extent than that of divalent-myristic-acid-siRNA. Cholesterol-siRNA may intercalate to cholesterol-rich lipid rafts[54] in the extracellular vesicle membrane, while divalent myristic acid may interact with lipid microdomains of higher fluidity, hence, facilitating release and/or RISC loading upon cellular uptake.

Extracellular vesicles failed to improve silencing activity of lipid-conjugated siRNAs in T cells, unlike in neurons[33, 37, 53]. These data suggest cell-type specific tropism of extracellular vesicles. Indeed, the cell of origin[55] as well as the membrane composition[33] has been shown to affect extracellular vesicle homing. Even though mesenchymal-stem-cell-derived vesicles have been shown to be taken up to T cells and impede their proliferation[56] or affect their differentiation[57], lymphoid-derived vesicles may show a more effective uptake[58]. We suggest that extracellular vesicles should only be used for siRNA delivery to T cells when a vesicle-intrinsic therapeutic add-on effect is expected, such as in graft-versus-host-disease[57].

Here we show potent uptake and silencing activity of lipid-conjugated siRNAs in human mononuclear immune cells. The utility of siRNAs have been demonstrated before in T cells including CAR-T cells[59]

and regulatory T cells[60], dendritic-cell-based vaccines[61, 62], macrophages[63], NK cells[64] and monocytes[65]. However, no systematic comparison of immune cell types and siRNA-delivering ligands has been carried out to date. Data presented here may be applied to deliver other types of oligonucleotides, such as CRISPR guide RNAs or antisense oligonucleotides (gapmer, splice-switching, RNA-editing etc.). Taken together, our results pave the way to future development of RNA-modified, RNA-potentiated or RNA-enabled cell therapies for cancer, autoimmune or alloimmune diseases.

Material and Methods

Oligonucleotides

Oligonucleotides[31] were a generous gift of Anastasia Khvorova, University of Massachusetts, Chan School of Medicine. The sequences and chemical modifications of oligonucleotides used in this work are listed in Supplementary Table 1.

PBMC isolation

Buffy coats were obtained from healthy donors from the Center of Clinical Transfusion Medicine Tuebingen. PBMCs were isolated from buffy coats by density gradient centrifugation. Briefly, the buffy coat bag was disinfected with 70% ethanol, buffy coats were then transferred to 50 ml conical tubes and diluted 1:1 with PBS (#D8537, Sigma). 35 ml of diluted buffy coat was then layered over 15 ml of Ficoll (#11768538, Fisher Scientific) and centrifuged at room temperature at 800 X g for 18 min without brake. The interphase containing PBMCs was transferred to 50 ml conical tubes, filled up to 50 ml with PBS and centrifuged at 450 X g for 5 min. Supernatant was aspirated and the pellet was resuspended in 40 ml PBS. This washing step was repeated two more times. Pellet was then resuspended in 40 ml PBS and centrifuged at 130 X g for 10 min (removal of platelets). Supernatant was then aspirated and pellet resuspended in RPMI-1640 medium (#392-0427, VWR) supplemented with 10% FBS (#11573397, Gibco), 1 % P/S (#P0781, Sigma), 25 mM Hepes (#9157.1, Carl Roth) and counted using trypan blue (#T8154, Sigma) and Neubauer hemocytometer (#631-0926, VWR).

T cell activation

1,5 x10^6 PBMCs were seeded in 1 ml RPMI-1640 medium (#392-0427, VWR) supplemented with 10% FBS (#11573397, Gibco), 1 % P/S (#P0781, Sigma), 25 mM Hepes (#9157.1, Carl Roth) in a 24-well cell culture plate (#10380932, Fisher Scientific). Loaded CD2/CD3/CD28 MACSiBeads (#130-091-441, Miltenyi Biotec) were added in a 1:2 bead-to-cell-ratio according to manufacturer's instructions and incubated for 3 days at 37°C, 5% CO_2. Medium was changed to ATC medium consisting of RPMI-1640 (#392-0427, VWR) with 10% FBS (#11573397, Gibco), 1% P/S (#P0781, Sigma), 25 mM Hepes (#9157.1, Carl Roth), 1 mM Sodiumpyruvat (#12539059, Gibco), 10 ng/ml IL-7 (#130-093-937, Miltenyi Biotec) and 3 ng/ml IL-15 (#130-093-955, Miltenyi Biotec).

Isolation of T cells, B cells, dendritic cells, natural killer cells and monocytes

Human T cells, B cells, dendritic cells, natural killer cells and monocytes were isolated from PBMCs by negative selection and magnetic sorting using cocktails of biotin-conjugated antibodies against non-target cells (#130-096-535,Miltenyi Biotec for T cells, (#130-101-638, Miltenyi Biotec for B cells, #130-100-777, Miltenyi Biotec for dendritic cells, #130-092-657, Miltenyi Biotec for natural killer cells, (#130-096-537, Miltenyi Biotec for monocytes). A QuadroMACS™ (Miltenyi Biotec) and LS columns (Miltenyi Biotec, Bergisch Gladbach, Germany) were used according to manufacturer's instructions. RPMI-1640 (#392-0427, VWR) with 10% FBS (#11573397, Gibco), 1% P/S (#P0781, Sigma), 25 mM Hepes (#9157.1, Carl Roth) and 1 mM Sodiumpyruvat (#12539059, Gibco) was supplemented with 10 ng/ml IL-7 (#130-093-937, Miltenyi Biotec) and 3 ng/ml IL-15 (#130-093-955, Miltenyi Biotec) for T cells, 10 ng/ml IL-4 (#130-093-920, Miltenyi Biotec) for B cells, 100 ng/ml GM-CSF (#130-093-864, Miltenyi Biotec) and 40 ng/ml IL-4 (#130-093-920, Miltenyi Biotec) for dendritic cells, 100 ng/ml IL-2 (#130-097-744, Miltenyi Biotec) for natural killer cells.

Differentiation of monocyte-derived dendritic cells and monocyte-derived macrophages

Monocytes were isolated as described above and $3x10^6$ cells/ml were plated in a 6-well plate using RPMI-1640 medium (#392-0427, VWR) supplemented with 10% FBS (#11573397, Gibco), 1% P/S (#P0781, Sigma), 25 mM Hepes (#9157.1, Carl Roth), 1 mM Sodiumpyruvat (#12539059, Gibco) and 14,3 µM β-mercaptoethanol (#10367100, Fisher Scientific). On day 0, 2 and 4 cytokines were added as followed: 20 ng/ml IL-4 (#130-093-920, Miltenyi Biotec) and 100 ng/ml GM-CSF (#130-093-864, Miltenyi Biotec) for monocyte-derived dendritic cells and 20 ng/ml IL-4 (#130-093-920, Miltenyi Biotec) and 40 ng/ml M-CSF (#130-096-485, Miltenyi Biotec) for monocyte-derived macrophages. On day 6, cells were collected with ice cold PBS and quality control was conducted by means of flow cytometry before using cells for downstream experiments.

Cell lines

Jurkat cells were cultured in RPMI-1640 medium (#392-0427, VWR) supplemented with 10% FBS (#11573397, Gibco), 1% P/S (#P0781, Sigma) and 25 mM Hepes (#9157.1, Carl Roth). Cells were passaged every 2 days to maintain a cell density between 1-3 $x10^6$ cells/ml.

NK-92-MI cells were cultured in RPMI-1640 medium (#392-0427, VWR) supplemented with 10% FBS (#11573397, Gibco), 1% P/S (#P0781, Sigma) and 25 mM Hepes (#9157.1, Carl Roth). Cells were passaged every 3 days to maintain a cell density of 0.5 $x10^6$ cells/ml.

Branched DNA assay

Cells were co-incubated with various concentrations of siRNA for 6 days at 37°C and 5% CO_2 in the presence of 5% FBS. Cells were then lysed and mRNA quantification was performed using QuantiGene™ Singleplex Assay kit, (Invitrogen™, Thermo Fisher Scientific) according to manufacturer's instructions. The following probesets were used: PPIB (siRNA target, SA-100 03, Invitrogen™, Thermo Fisher Scientific), HPRT, housekeeping in PBMC, ATC, NK, macrophages, dendritic cells SA-100 30, Invitrogen™, Thermo Fisher Scientific) and RAN (housekeeping in Jurkats, B cells, monocytes, NK92-MI, SA-15837, Invitrogen™, Thermo Fisher Scientific). The linear range of this assay

was identified for each probeset in each cell type. Datasets were first normalized to housekeeping gene expression and afterwards to untreated control. Each measurement was performed in triplicates.

Isolation of small extracellular vesicles

Small extracellular vesicles (sEVs) were isolated from umbilical cord matrix derived mesenchymal stem cells (#C-12971, PromoCell)) via differential ultracentrifugation. Briefly, cells were cultivated in mesenchymal stem cell growth medium 2 (#C-28009, PromoCell). Medium was changed to RPMI-1640 (#392-0427, VWR) without FBS or antibiotics 24 hours before sEV isolation. After 24hours, this serum-free conditioned medium was collected and mesenchymal stem cell growth medium 2 (#C-28009, PromoCell) added to cells for further cultivation. Conditioned medium was centrifuged at 300 X g, for 10 min at room temperature to remove dead cells. Supernatant was then centrifuged at 10,000 X g for 30 min at 4°C and filtered through a 0,2 µm membrane (Nalgene® bottle-top sterile filter, Z35223, Sigma). Small extracellular vesicles were pelleted at 100,000 X g for 1,5 h at 4°C by using Ti-45 rotor (Beckman Coulter) and 70 ml polycarbonate bottles (Beckman Coulter) in a Sorvall™ WX Ultra Series ultracentrifuge (Thermo Fisher). Pellets were pooled in 1 ml PBS and centrifuged at 100,000 X g for 1,5 h at 4°C in 1,5 ml tubes in a Ti-45 rotor (Beckman Coulter) using adapters (#11004, Beranek). Final pellet was resuspended in 100 µl PBS and frozen in a 0,1M sucrose with a protease inhibitor cocktail (cOmplete™, Mini, #11836170001, Roche).

siRNAs were co-incubated with sEVs (siRNA-to-EV ratio 10.000:1) for one hour at 37°C at 5% CO_2. Then loaded sEVs were pelleted at 100,000 g for 90 minutes at 4°C and unloaded siRNA discarded. siRNA-loaded sEV pellet was then resuspended in cell culture medium and added to cells.

Formulation of lipid nanoparticles

Lipid nanoparticles (LNPs) were formulated using NanoAssemblr® Spark™ instrument (Precision NanoSystems) and GenVoy-ILM™ T cell kit for mRNA (Precision NanoSystems) according to manufacturer's instructions. 10 µg siRNA (around 800 pmol) were added to the hydrous phase during LNP production.

Characterization of extracellular vesicles and lipid nanoparticles

Nanoparticle Tracking Analysis was performed to determine concentration and size distribution of sEVs and LNPs using a NanoSight NS300 (Malvern) instrument. Samples were infused using continuous syringe flow pump (infusion rate 800) and 30 second movies captured 3 times at 20°C. Detection threshold was set at 5. sEVs and LNPs were appropriately diluted in PBS prior to measurement to have 20-120 particles per frame and more than 1000 valid particles in total in order to ensure robust analysis. Zeta potential as an indicator for colloidal stability was measured by Zetasizer Nano (Malvern) with a disposable folded capillary (DTS1070) using Smoluchowski calculation. sEVs and LNPs were diluted 1:500 in PBS prior to measurement with following settings: Dispersant PBS (Viscosity: 1,0041 cP; RI: 1,330; Dielectric constant 79,0), 20°C, equilibration time 120 s and DTS 1070 cell.

Flow cytometry

Flow cytometry was performed using a FACS Canto II instrument (BD Biosciences). Briefly, cells were harvested via centrifugation, then blocked with human IgG (#I4506 Sigma) for 10 minutes at 4°C, washed, then stained with live/dead stain and fluorophore-conjugated antibodies according to manufacturer;s instructions. Following antibodies were obtained from Biolegend: anti-CD3 (#300317, #317343), anti-CD4 (#300514), anti-CD8 (#300933), anti-CD19 (#363005). Antibodies against CD14 (#130-110-583) and HLA-DR (#130-111-943) were obtained from Miltenyi Biotec. Dapi (#422801, Biolegend) and Zombie NIR (#423105, Biolegend) were used to stain dead cells. PBS (#D8537, Sigma) supplemented with 0,5% BSA (#9400.1, Carl Roth) and 2 mM EDTA (#A4892,0100, PanReac AppliChem) was used as buffer. Data were analyzed with FlowJo 10.8.0 (Tree Star).

Microscopy

Dendritic cells were isolated via negative selection from frozen PBMCs as described above. $5x10^5$ cells were seeded in a 96-well U-bottom plate (#10344311, Fisher Scientific) in 100 µl medium consisting of RPMI-1640 (#392-0427, VWR) with 10% FBS (#11573397, Gibco), 1% P/S (#P0781, Sigma), 100 ng/ml GM-CSF (#130-093-864, Miltenyi Biotec) and 40 ng/ml IL-4 (#130-093-920, Miltenyi Biotec), treated

with 1 µM final concentration siRNA and incubated at 37°C, 5% CO_2. Cells were then washed by centrifugation at 400 X g, 5 min at room temperature and resuspended in 150 µl PBS (#D8537, Sigma). Funnel, filter card (#5991022, Thermo Scientific) and microscope slide (#235504006, DWK Life Sciences) were assembled in the centrifuge (Cytospin 4, Thermo Scientific), filled with cell suspension and centrifuged at 250 rpm for 10 min. A round circle was drawn around the cell spot with a Pap-Pen (#Z377821, Sigma-Aldrich). Cells were then fixed with 4 % Paraformaldehyde (#15424389, Fisher Scientific) for 10 min at room temperature and rinsed 3 times with PBS (#D8537, Sigma). Fixed cells were stained with 1 ng/ml Dapi (#422801, Biolegend) in PBS for 10 min at room temperature in the dark and washed 3 times with PBS (#D8537, Sigma). PBS was completely removed and cells were left to dry for 5 min at room temperature. Dry cells were mounted with 1 drop of Fluoromount-G™ (#15586276, Invitrogen, Fisher Scientific), covered with cover slide (#4818602, Param GmbH) and dried overnight at room temperature in the dark. Fluorescent images were acquired using ApoTome 2 (Zeiss). Images were analyzed using Fiji (Version 2.11). Fluorescence was quantified using the pixel integrated density method.

Statistical analysis

Silencing data was analyzed in Prism Version 9.4.1. (GraphPad). Silencing curves were fit using the "log(inhibitor) vs. response (three parameters)" function. Curves were compared using two-way ANOVA with multiple comparison tests.

Data Availability Statement

The authors confirm that the data supporting the findings of this study are available within the article and its supplementary materials.

Acknowledgements

We thank Annabelle Biscans, Dimas Echeverria and Anastasia Khvorova (University of Massachusetts Medical School) for providing the oligonucleotides used in this study. We thank the FACS Core Facility, University Hospital Tübingen for assistance with flow cytometric measurements. We thank Olga

Oleksiuk (German Center for Neurodegenerative Diseases, Tübingen Site) for assistance with fluorescent imaging. We thank Philipp Schaible and Clemens Lochmann for initial assistance with QuantiGene assay establishment. We thank Emmanuelle Ribeiro for assistance with establishing PBMC isolation and primary T cell cultures. We thank Thomas Gasser (Hertie Institute, Tübingen) for access to NanoSight instrument and Philipp Bucher for initial assistance with measurements. We thank Andreas Kappler (Department of Geoscience, University of Tübingen) for access to Zetasizer and Lars Grimm for initial assistance with measurements. This work was supported by the German Cancer Aid [70113948 to R.A.H.); and the Faculty of Medicine, University of Tübingen [473-0-0 to R.A.H., 2652-0-0 to R.A.H.].

Author Contributions

Conceptualization A.K., R.A.H. Methodology A.K., T.R., R.A.H. Investigation A.K. Writing – Original Draft A.K., R.A.H. Visualization A.K., R.A.H. Supervision R.A.H. Project Administration R.A.H. Funding Acquisition R.A.H.

Declaration of Interest

Authors of this manuscript have a pending patent related to nucleic-acid-modified cell therapies.

Keywords

siRNA, delivery, extracellular vesicle, lipid conjugate, immunotherapy

References

1. Liu, D., et al., *A practical guide to the monitoring and management of the complications of systemic corticosteroid therapy.* Allergy Asthma Clin Immunol, 2013. **9**(1): p. 30.
2. McMullen, J.R., et al., *Ibrutinib increases the risk of atrial fibrillation, potentially through inhibition of cardiac PI3K-Akt signaling.* Blood, 2014. **124**(25): p. 3829-30.
3. Honigberg, L.A., et al., *The Bruton tyrosine kinase inhibitor PCI-32765 blocks B-cell activation and is efficacious in models of autoimmune disease and B-cell malignancy.* Proc Natl Acad Sci U S A, 2010. **107**(29): p. 13075-80.
4. Giménez, N., et al., *Targeting IRAK4 disrupts inflammatory pathways and delays tumor development in chronic lymphocytic leukemia.* Leukemia, 2020. **34**(1): p. 100-114.
5. Castillo, J.J., et al., *Novel approaches to targeting MYD88 in Waldenström macroglobulinemia.* Expert Rev Hematol, 2017. **10**(8): p. 739-744.

6. Liu, C., et al., *LINC00987 knockdown inhibits the progression of acute myeloid leukemia by suppressing IGF2BP2-mediated PA2G4 expression.* Anticancer Drugs, 2022. **33**(1): p. e207-e217.
7. Iwamura, K., et al., *siRNA-mediated silencing of PD-1 ligands enhances tumor-specific human T-cell effector functions.* Gene Ther, 2012. **19**(10): p. 959-66.
8. Freeley, M., et al., *RNAi Screening with Self-Delivering, Synthetic siRNAs for Identification of Genes That Regulate Primary Human T Cell Migration.* J Biomol Screen, 2015. **20**(8): p. 943-56.
9. Ligtenberg, M.A., et al., *Self-Delivering RNAi Targeting PD-1 Improves Tumor-Specific T Cell Functionality for Adoptive Cell Therapy of Malignant Melanoma.* Mol Ther, 2018. **26**(6): p. 1482-1493.
10. Herrmann, A., et al., *CTLA4 aptamer delivers STAT3 siRNA to tumor-associated and malignant T cells.* J Clin Invest, 2014. **124**(7): p. 2977-87.
11. Berezhnoy, A., et al., *Aptamer-targeted inhibition of mTOR in T cells enhances antitumor immunity.* J Clin Invest, 2014. **124**(1): p. 188-97.
12. Song, E., et al., *Antibody mediated in vivo delivery of small interfering RNAs via cell-surface receptors.* Nat Biotechnol, 2005. **23**(6): p. 709-17.
13. Bäumer, N., et al., *Targeted siRNA nanocarrier: a platform technology for cancer treatment.* Oncogene, 2022. **41**(15): p. 2210-2224.
14. Peer, D., et al., *Selective gene silencing in activated leukocytes by targeting siRNAs to the integrin lymphocyte function-associated antigen-1.* Proceedings of the National Academy of Sciences, 2007. **104**(10): p. 4095-4100.
15. Kumar, P., et al., *T Cell-Specific siRNA Delivery Suppresses HIV-1 Infection in Humanized Mice.* Cell, 2008. **134**(4): p. 577-586.
16. Lokugamage, M.P., et al., *Constrained Nanoparticles Deliver siRNA and sgRNA to T Cells In Vivo without Targeting Ligands.* Adv Mater, 2019. **31**(41): p. e1902251.
17. Khvorova, A. and J.K. Watts, *The chemical evolution of oligonucleotide therapies of clinical utility.* Nat Biotechnol, 2017. **35**(3): p. 238-248.
18. Hong, D.S., et al., *Phase 1 study of MRX34, a liposomal miR-34a mimic, in patients with advanced solid tumours.* British Journal of Cancer, 2020. **122**(11): p. 1630-1637.
19. Adams, D., et al., *Patisiran, an RNAi Therapeutic, for Hereditary Transthyretin Amyloidosis.* New England Journal of Medicine, 2018. **379**(1): p. 11-21.
20. Hassler, M.R., et al., *Comparison of partially and fully chemically-modified siRNA in conjugate-mediated delivery in vivo.* Nucleic Acids Res, 2018. **46**(5): p. 2185-2196.
21. Ly, S., et al., *Single-Stranded Phosphorothioated Regions Enhance Cellular Uptake of Cholesterol-Conjugated siRNA but Not Silencing Efficacy.* Mol Ther Nucleic Acids, 2020. **21**: p. 991-1005.
22. Van Hoeck, J., et al., *Non-viral siRNA delivery to T cells: Challenges and opportunities in cancer immunotherapy.* Biomaterials, 2022. **286**(121510): p. 121510.
23. Mulder, W.J.M., et al., *Therapeutic targeting of trained immunity.* Nat Rev Drug Discov, 2019. **18**(7): p. 553-566.
24. Ureña-Bailén, G., et al., *Preclinical Evaluation of CRISPR-Edited CAR-NK-92 Cells for Off-the-Shelf Treatment of AML and B-ALL.* Int J Mol Sci, 2022. **23**(21).
25. Sloas, C., S. Gill, and M. Klichinsky, *Engineered CAR-Macrophages as Adoptive Immunotherapies for Solid Tumors.* Front Immunol, 2021. **12**(783305): p. 783305.
26. Gabitova, L., et al., *318 Pre-clinical development of a CAR monocyte platform for cancer immunotherapy.* Journal for ImmunoTherapy of Cancer, 2022. **10**(Suppl 2): p. A334.
27. Liau, L.M., et al., *Association of Autologous Tumor Lysate-Loaded Dendritic Cell Vaccination With Extension of Survival Among Patients With Newly Diagnosed and Recurrent Glioblastoma: A Phase 3 Prospective Externally Controlled Cohort Trial.* JAMA Oncology, 2023. **9**(1): p. 112-121.
28. Huang, M.N., et al., *Antigen-loaded monocyte administration induces potent therapeutic antitumor T cell responses.* J Clin Invest, 2020. **130**(2): p. 774-788.

29. Labanieh, L. and C.L. Mackall, *CAR immune cells: design principles, resistance and the next generation.* Nature, 2023. **614**(7949): p. 635-648.
30. Odak, I., et al., *Spectral flow cytometry cluster analysis of therapeutic donor lymphocyte infusions identifies T cell subsets associated with outcome in patients with AML relapse.* Front Immunol, 2022. **13**(999163): p. 999163.
31. Biscans, A., et al., *The valency of fatty acid conjugates impacts siRNA pharmacokinetics, distribution, and efficacy in vivo.* J Control Release, 2019. **302**: p. 116-125.
32. McKinlay, C.J., et al., *Enhanced mRNA delivery into lymphocytes enabled by lipid-varied libraries of charge-altering releasable transporters.* Proceedings of the National Academy of Sciences, 2018. **115**(26): p. E5859-E5866.
33. Haraszti, R.A., et al., *Serum Deprivation of Mesenchymal Stem Cells Improves Exosome Activity and Alters Lipid and Protein Composition.* iScience, 2019. **16**: p. 230-241.
34. Haraszti, R.A., et al., *5′-Vinylphosphonate improves tissue accumulation and efficacy of conjugated siRNAs in vivo.* Nucleic Acids Res, 2017. **45**(13): p. 7581-7592.
35. Biscans, A., et al., *Hydrophobicity of Lipid-Conjugated siRNAs Predicts Productive Loading to Small Extracellular Vesicles.* Mol Ther, 2018. **26**(6): p. 1520-1528.
36. Zimmermann, T.S., et al., *RNAi-mediated gene silencing in non-human primates.* Nature, 2006. **441**(7089): p. 111-4.
37. Didiot, M.C., et al., *Exosome-mediated Delivery of Hydrophobically Modified siRNA for Huntingtin mRNA Silencing.* Mol Ther, 2016. **24**(10): p. 1836-1847.
38. Billingsley, M.M., et al., *Ionizable Lipid Nanoparticle-Mediated mRNA Delivery for Human CAR T Cell Engineering.* Nano Letters, 2020. **20**(3): p. 1578-1589.
39. Kordelas, L., et al., *MSC-derived exosomes: a novel tool to treat therapy-refractory graft-versus-host disease.* Leukemia, 2014. **28**(4): p. 970-3.
40. Aliotta, J.M., et al., *Exosomes induce and reverse monocrotaline-induced pulmonary hypertension in mice.* Cardiovasc Res, 2016. **110**(3): p. 319-30.
41. Badri, P., et al., *Pharmacokinetic and Pharmacodynamic Properties of Cemdisiran, an RNAi Therapeutic Targeting Complement Component 5, in Healthy Subjects and Patients with Paroxysmal Nocturnal Hemoglobinuria.* Clin Pharmacokinet, 2021. **60**(3): p. 365-378.
42. Spector, A.A. and M.A. Yorek, *Membrane lipid composition and cellular function.* Journal of Lipid Research, 1985. **26**(9): p. 1015-1035.
43. Osborn, M.F., et al., *Hydrophobicity drives the systemic distribution of lipid-conjugated siRNAs via lipid transport pathways.* Nucleic Acids Res, 2019. **47**(3): p. 1070-1081.
44. Wolfrum, C., et al., *Mechanisms and optimization of in vivo delivery of lipophilic siRNAs.* Nat Biotechnol, 2007. **25**(10): p. 1149-57.
45. Ly, S., et al., *Visualization of self-delivering hydrophobically modified siRNA cellular internalization.* Nucleic Acids Res, 2017. **45**(1): p. 15-25.
46. Wang, B., et al., *Protein N-myristoylation: functions and mechanisms in control of innate immunity.* Cellular & Molecular Immunology, 2021. **18**(4): p. 878-888.
47. Zhu, Y., et al., *Heme Oxygenase 2 Binds Myristate to Regulate Retrovirus Assembly and TLR4 Signaling.* Cell Host Microbe, 2017. **21**(2): p. 220-230.
48. Gorska, M.M., et al., *Unc119, a novel activator of Lck/Fyn, is essential for T cell activation.* J Exp Med, 2004. **199**(3): p. 369-79.
49. Bietz, A., et al., *Cholesterol Metabolism in T Cells.* Frontiers in Immunology, 2017. **8**.
50. Semple, S.C., et al., *Rational design of cationic lipids for siRNA delivery.* Nat Biotechnol, 2010. **28**(2): p. 172-6.
51. Jayaraman, M., et al., *Maximizing the potency of siRNA lipid nanoparticles for hepatic gene silencing in vivo.* Angew Chem Int Ed Engl, 2012. **51**(34): p. 8529-33.
52. Brown, C.R., et al., *Investigating the pharmacodynamic durability of GalNAc-siRNA conjugates.* Nucleic Acids Res, 2020. **48**(21): p. 11827-11844.
53. Haraszti, R.A., et al., *Optimized Cholesterol-siRNA Chemistry Improves Productive Loading onto Extracellular Vesicles.* Mol Ther, 2018. **26**(8): p. 1973-1982.

54. Lingwood, D. and K. Simons, *Lipid rafts as a membrane-organizing principle.* Science, 2010. **327**(5961): p. 46-50.
55. Hoshino, A., et al., *Tumour exosome integrins determine organotropic metastasis.* Nature, 2015. **527**(7578): p. 329-35.
56. Lee, S., et al., *Mesenchymal stem cell-derived exosomes suppress proliferation of T cells by inducing cell cycle arrest through p27kip1/Cdk2 signaling.* Immunol Lett, 2020. **225**: p. 16-22.
57. Zhang, B., et al., *Mesenchymal stromal cell exosome-enhanced regulatory T-cell production through an antigen-presenting cell-mediated pathway.* Cytotherapy, 2018. **20**(5): p. 687-696.
58. Gutiérrez-Vázquez, C., et al., *Transfer of extracellular vesicles during immune cell-cell interactions.* Immunol Rev, 2013. **251**(1): p. 125-42.
59. Schaible, P., et al., *RNA Therapeutics for Improving CAR T-cell Safety and Efficacy.* Cancer Res, 2023. **83**(3): p. 354-362.
60. Raffin, C., L.T. Vo, and J.A. Bluestone, *Treg cell-based therapies: challenges and perspectives.* Nat Rev Immunol, 2020. **20**(3): p. 158-172.
61. Zhang, Y., et al., *A new cancer immunotherapy via simultaneous DC-mobilization and DC-targeted IDO gene silencing using an immune-stimulatory nanosystem.* Int J Cancer, 2018. **143**(8): p. 2039-2052.
62. Zheng, X., et al., *Silencing IDO in dendritic cells: a novel approach to enhance cancer immunotherapy in a murine breast cancer model.* Int J Cancer, 2013. **132**(4): p. 967-77.
63. Uehara, K., et al., *Targeted delivery to macrophages and dendritic cells by chemically modified mannose ligand-conjugated siRNA.* Nucleic Acids Res, 2022. **50**(9): p. 4840-4859.
64. Palacios, D., et al., *An optimized platform for efficient siRNA delivery into human NK cells.* Eur J Immunol, 2022. **52**(7): p. 1190-1193.
65. Troegeler, A., et al., *An efficient siRNA-mediated gene silencing in primary human monocytes, dendritic cells and macrophages.* Immunol Cell Biol, 2014. **92**(8): p. 699-708.

List of Figure Captions

Figure 1 Lipid conjugates mediate efficient siRNA uptake in immune cells

Lipid-conjugated, fluorescently labeled, fully chemically modified siRNAs (1µM) were co-incubated with cells for 24 hours. siRNA uptake was estimated based on siRNA fluorescence (Cy3) in living cells via flow cytometry. Unconjugated siRNA (black) as well as cholesterol conjugated (grey), monovalent myristic acid conjugated (blue) and divalent myristic acid conjugated (magenta) showed uptake across human cell types tested: Jurkat T cell line (A), peripheral blood mononuclear cells lymphocyte fraction (B), activated T cells (C), B cells (D), natural killer cells (E), dendritic cells (F), monocytes (G), monocyte-derived dendritic cells (H) and monocyte-derived macrophages (I). Primary cells (B-I) were isolated from buffy coats of healthy donors via a combination of density centrifugation, negative selection and interleukin-driven differentiation. Dashed lines mark the mode of fluorescence intensity of the siRNA showing the best uptake in each cell type.

Figure 2 Lipid conjugate and target cell type interact to mediate siRNA silencing

Lipid-conjugated (cholesterol grey, monovalent myristic acid blue, divalent myristic acid magenta, unconjugated black), fully chemically modified siRNAs were co-incubated with cells in increasing concentrations for 6 days. Target mRNA (PPIB) expression was measured via QuantiGene® assay in Jurkat T cell line (A), peripheral blood mononuclear cells (B), activated T cells (C), B cells (D), natural killer cells (E), dendritic cells (F), monocytes (G), monocyte-derived dendritic cells (H) and monocyte-derived macrophages (I). Primary cells (B-I) were isolated from buffy coats of healthy donors via a combination of density centrifugation, negative selection and interleukin-driven differentiation. N=3-6,

average±SEM. Silencing was modeled using "log(inhibitor) vs. response (three parameters)" function in prism and corresponding IC50 values depicted in (J).

Figure 3 Uptake kinetics of lipid conjugated siRNAs in T cells

Fluorescently labeled (Cy3) cholesterol-siRNA (grey), divalent-myristic-acid-siRNA (magenta) or unconjugated siRNAs (black) was added to Jurkat cells (A), PBMCs (B) or activated T cells (C) and Cy3 fluorescence analyzed in living cells via flow cytometry upon a series of incubation times. N=2 measurements of 50.000 cells each, average±SEM

Figure 4 Intracellular localization of lipid-conjugated siRNA in dendritic cells

Dendritic cells were treated with unconjugated siRNA (black), cholesterol-siRNA (grey) or divalent-myristic acid siRNA (magenta) and fixed after different incubation times. siRNA fluorescence (Cy3, in red) and nuclei (Dapi, blue) were imaged on an ApoTome2 microscope (A). Cy3 fluorescence was quantified used the pixel integrated density method in Fiji (B). N=5 images, average±SEM.

Figure 5 Conjugate mediate siRNA delivery outperforms nanoparticle mediated delivery in T cells

Human primary activated T cells obtained from buffy coats of healthy donors were co-incubated with cholesterol- (A) monovalent myristic acid – (B) and divalent myristic acid – (C) conjugated siRNA either unformulated (black) or formulated in lipid nanoparticle (brown)s or small extracellular vesicles (green). Lipid nanoparticles encapsulating lipid-conjugated siRNA were produced using a microfluidic system and a lipid mixture specific to T cell delivery (ref). Small extracellular vesicles (sEVs) were enriched from supernatant of umbilical cord Wharton´s jelly derived mesenchymal stem cell supernatants via differential ultracentrifugation. sEVs were then co-incubated with lipid-conjugated siRNA for 1 hour at 37C and unloaded siRNA removed via ultracentrifugation (ref). Target mRNA (PPIB) expression was measured via QuantiGene® assay. N=3, average±SEM

Figure 1

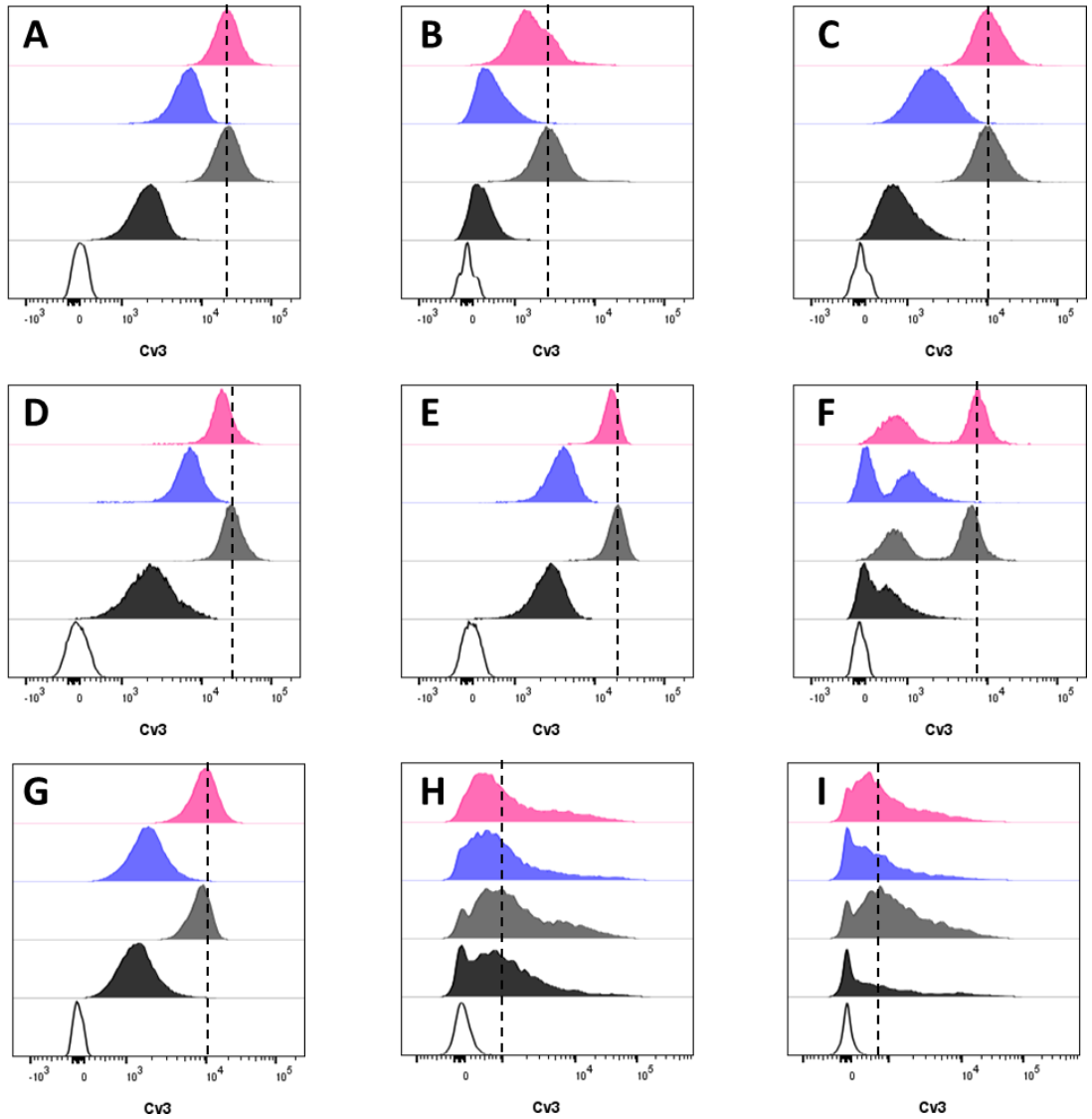

Figure 2

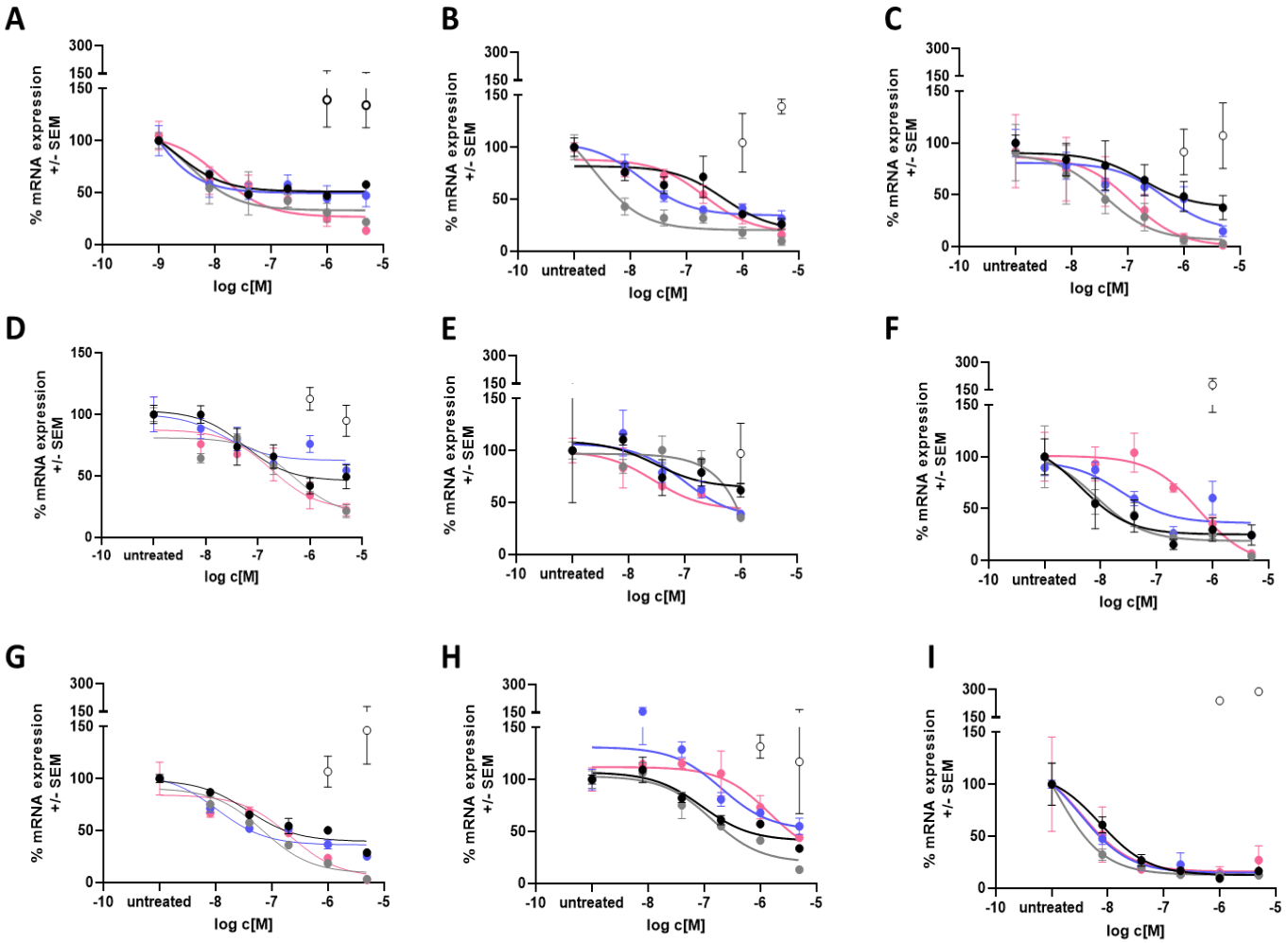

J

IC50 in nM	Jurkat	PBMCs	activated T cells	B cells	NK	DCs	monocytes	monocyte derived DCs	monocyte derived macrophages	NK-92-MI
unconjugated	2	468,5	187,4	55	1089	4,5	37,6	92,3	7,3	34,8
monovalent myristic acid	0,5	16,3	461,4	23,9	77,6	24,1	10,5	205,4	3,3	40,4
cholesterol	3,5	2,2	40,2	481,7	n/a	8,1	69,9	136,5	1,1	59,2
divalent myristic acid	12,3	211,2	116	181,9	465,7	573,4	214,3	1468	3,5	246

Figure 3

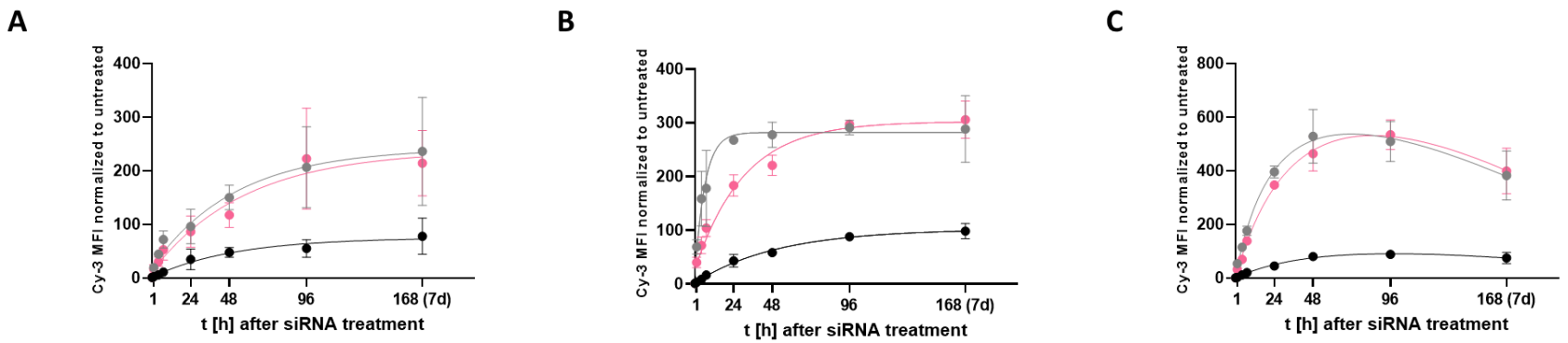
A
B
C
Cy-3 MFI normalized to untreated
t [h] after siRNA treatment
1
24
48
96
168 (7d)
0
100
200
300
400
600
800

Figure 4

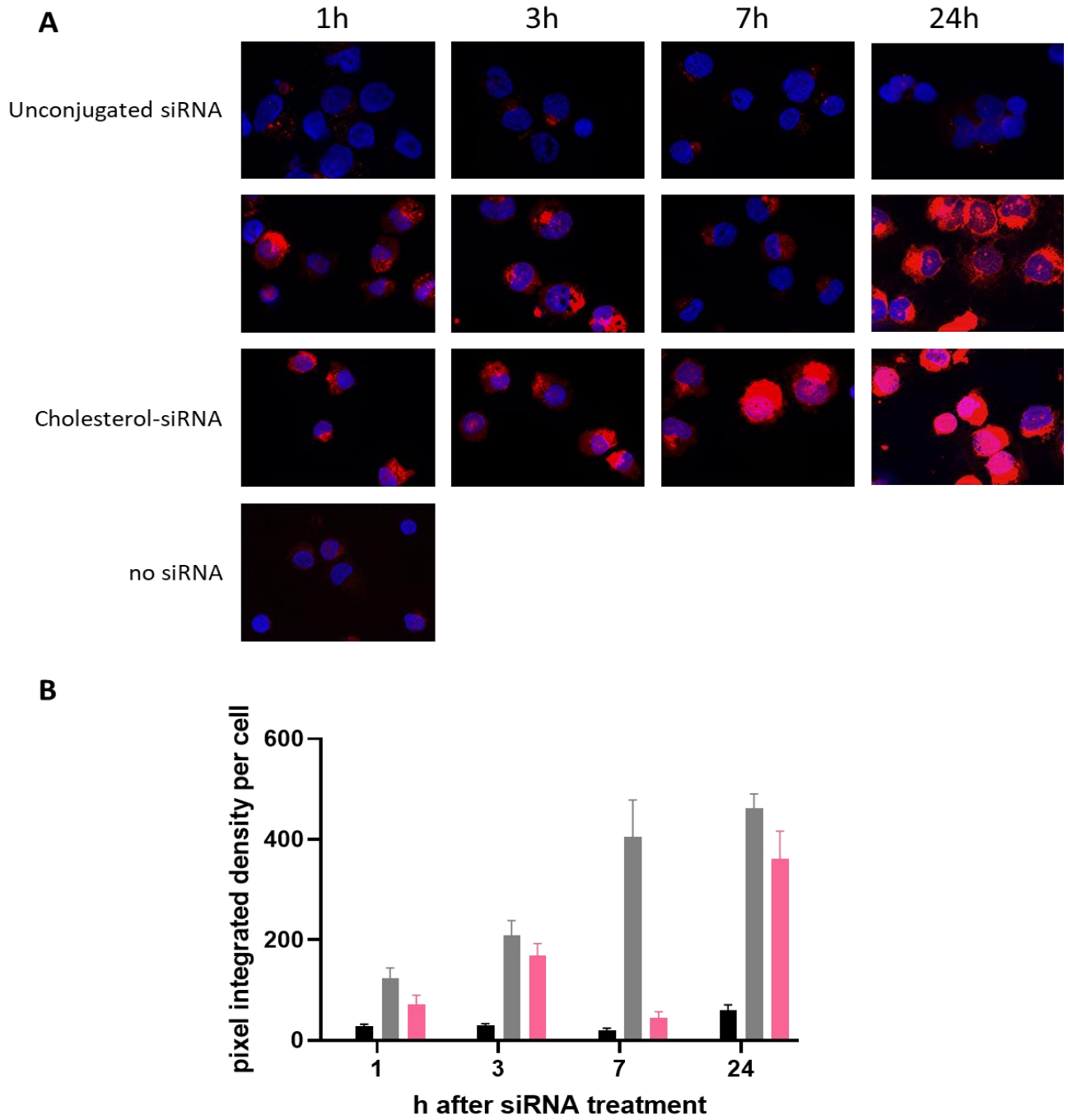
A
1h
3h
7h
24h
Unconjugated siRNA
Cholesterol-siRNA
no siRNA
B
pixel integrated density per cell
600
400
200
0
1
3
7
24
h after siRNA treatment

Figure 5

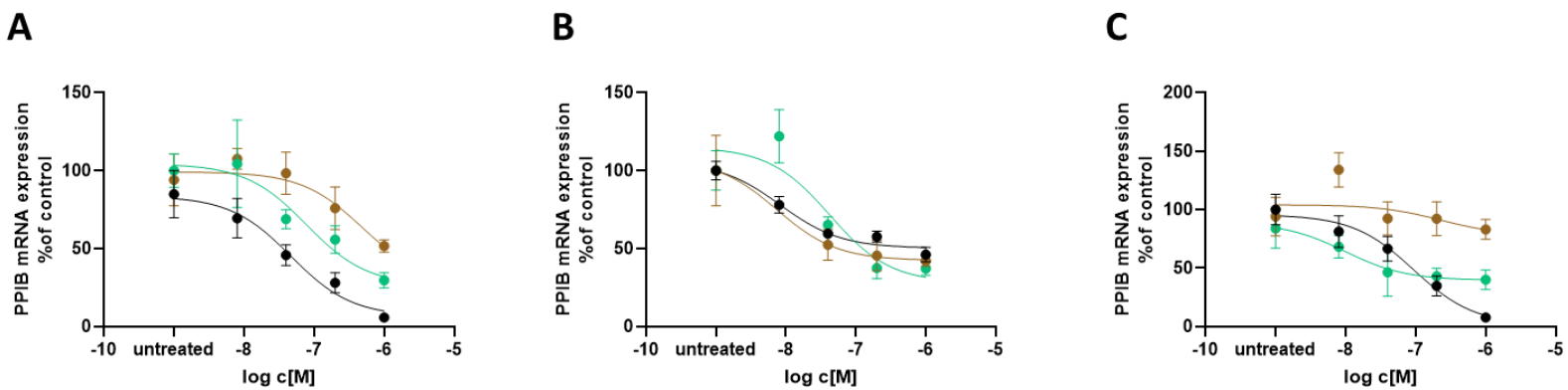
A
B
C
PPIB mRNA expression
%of control
150
100
50
0
200
-10
untreated
-8
-7
-6
-5
log c[M]

supplement

target		sequence
NTC	antisense	P(mU)#(fA)#(mA)(mU)(mC)(fG)(mU)(mA)(mU)(mU)(mU)(mG)(mU)#(fC)#(mA)#(fA)#(mU)#(mC)#(mA)#(fU)
	sense	(mU)#(mG)#(mA)(mC)(fA)(fA)(fA)(mU)(fA)(mC)(mG)(mA)(mU)#(mU)#(mA)-cholesterol
PPIB	antisense	V(mU)#(fC)#(mA)(fC)(mG)(fA)(mU)(fG)(mG)(fA)(mA)(fU)(mU)#(fU)#(mG)#(fC)#(mU)#(fG)#(mU)#(fU)
	sense	Cy3-(fC)#(mA)#(fA)(mA)(fU)(mU)(fC)(mC)(fA)(mU)(fC)(mG)(fU)#(mG)#(fA)-lipid conjugate

acronym	
V	5´-(E)-Vinylphosphonate
#	Phosphorothioate linkage
m	2´-O-methyl
f	2´-fluoro
Cy3	Cyanine-3

Supplementary Table 1. Oligonucleotide sequences and their chemical modifications used in this study

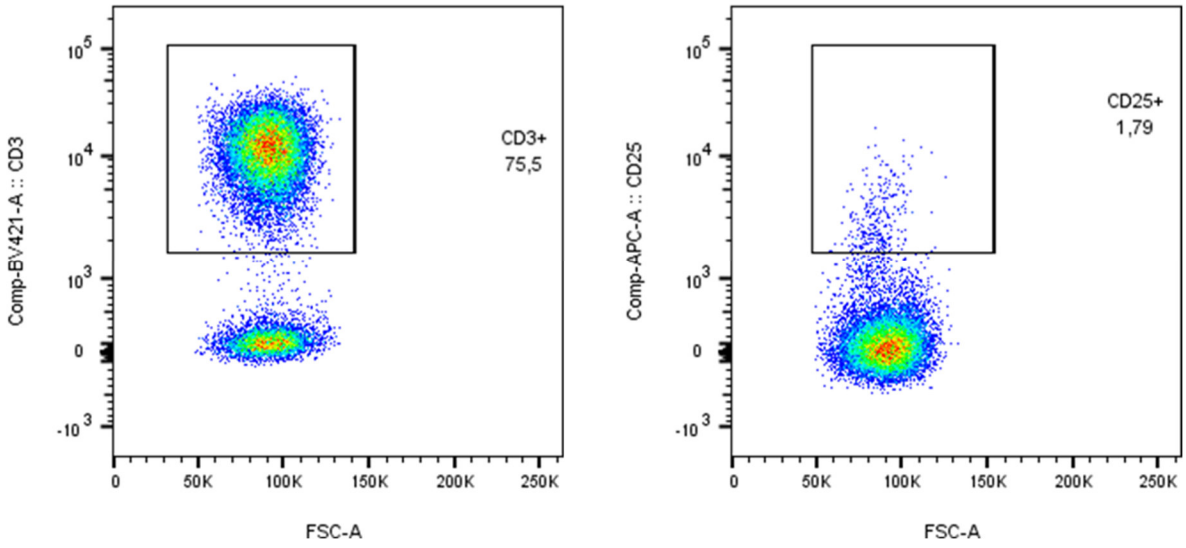

Supplementary Figure 1 Representative flow cytometric analysis of PBMCs
Peripheral blood mononuclear cells were stained for CD3 (T cell marker) and CD25 (activation) and live cells analyzed. Lymphocyte gate was set based on characteristic forward and side scatters. 76% (on the left) of all lymphocytes were T cells, and 98% (on the right) of dose lacked the activation marker CD25, hence, could be described as resting.

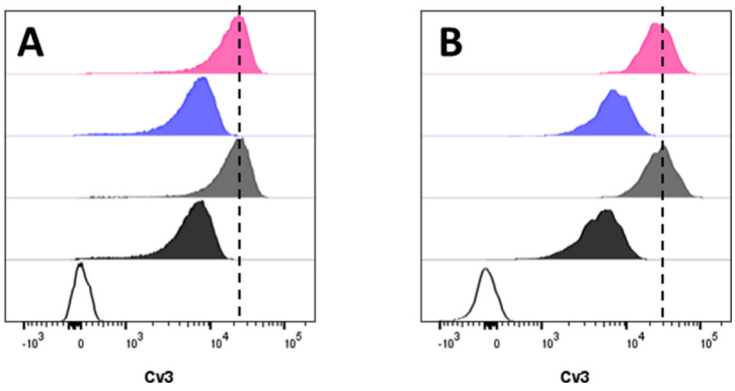

Supplementary Figure 2 Lipid-conjugated siRNA uptake into therapeutic cell types

Lipid-conjugated, fluorescently labeled, fully chemically modified siRNAs (1µM) were co-incubated with cells for 24 hours. siRNA uptake was estimated based on siRNA fluorescence (Cy3) in living cells via flow cytometry. Unconjugated siRNA (black) as well as cholesterol conjugated (grey), monovalent myristic acid conjugated (blue) and divalent myristic acid conjugated (magenta) showed uptake across human cell types tested: NK-92-MI (A), CD19-CAR-T cells (B).

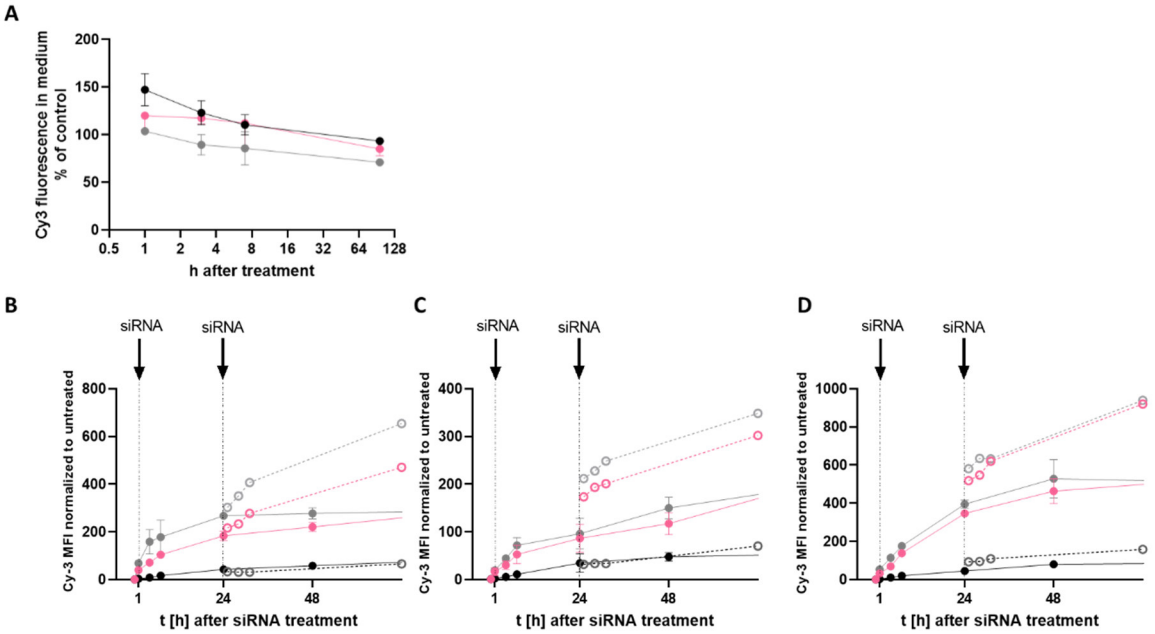

Supplementary Figure 3 Lipid-conjugated siRNA uptake kinetic into human T cells

Fluorescently labeled (Cy3) cholesterol-siRNA (grey), divalent-myristic-acid-siRNA (magenta) or unconjugated siRNAs (black) was added to cells, and incubated for varying times. Cell suspensions were then centrifuged and samples of cell-free conditioned medium transferred to 96-well-plates. Cy3-fluoresence was then measured using a fluorescent plate reader (Infinite® 200 Pro M-Plex, Tecan) (A). Cy3 fluorescence was also analyzed in Jurkat cells (B), PBMCs (C) or activated T cells (D) via flow cytometry. siRNA treatment (1 µM each) are indicated via arrows. Full dots indicate measurements of cells with one siRNA treatment at timepoint 0. Empty dots indicate measurements of cells with two siRNA treatments, at timepoint 0 and 24 hours later.

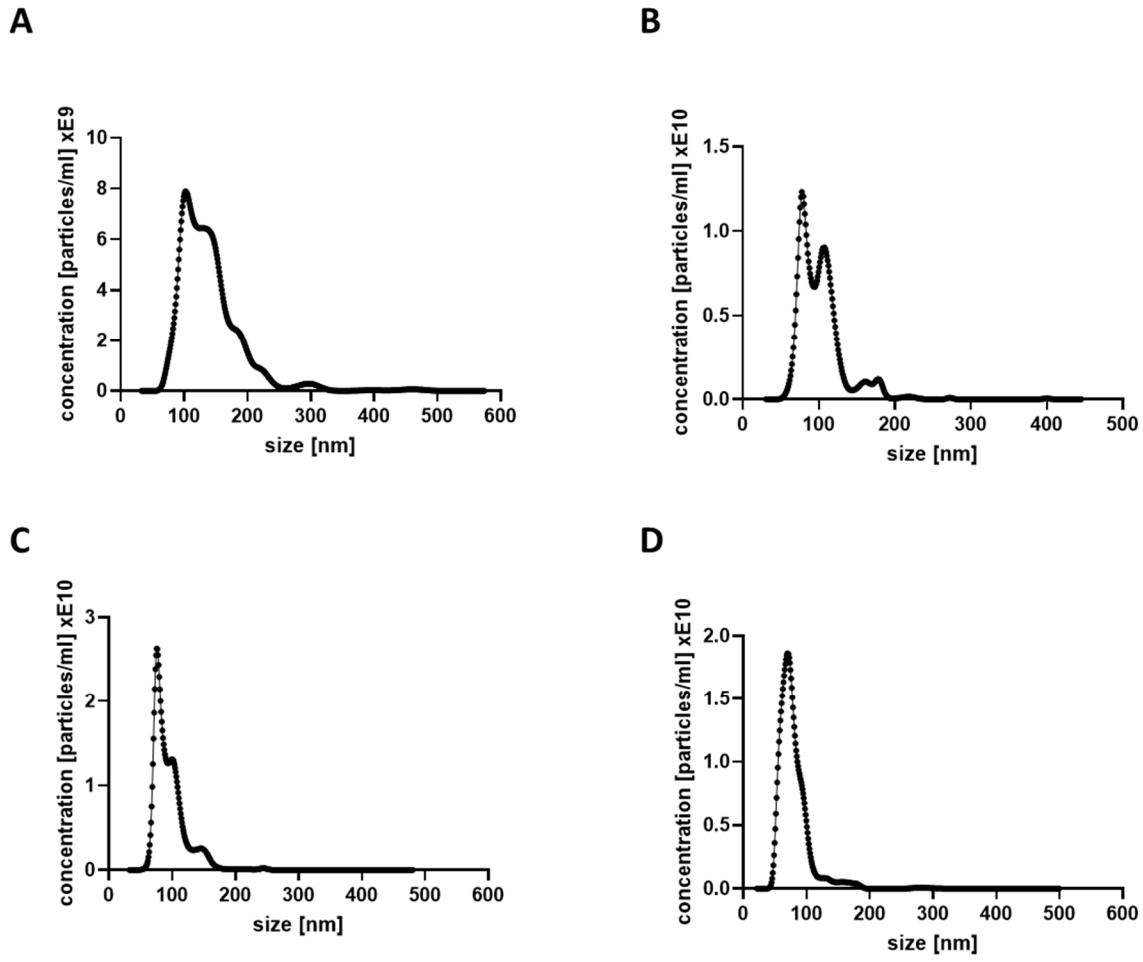

E

	Zeta potential [mV]
MSC-derived small extracellular vesicles	-18.1
cholesterol-siRNA LNP	-10.93
monovalent-myristic-acid-siRNA LNP	-5.35
divalent-myristic-acid-siRNA LNP	-3.77

Supplementary Figure 4 Characterization of nanoparticles

Small extracellular vesicles (A) were purified from umbilical cord matrix mesenchymal stem cells via differential ultracentrifugation. Lipid nanoparticles were produced on a NanoAssemplr Spark instrument with either cholesterol-siRNA (B), monovalent-myristic-acid-siRNA (C), or divalent-myristic-acid-siRNA (D). The particle size was assessed via nanoparticle tracking analysis on a NanoSight instrument (A-D). Nanoparticle charge was assessed using a Zetasizer (E).